Bioelectromagnetics 25:620–630 (2004)

Magnetic Resonances of Ions in Biological Systems

Stefan Engström[1]* and Joseph D. Bowman[2]

[1]*Department of Neurology, Vanderbilt University Medical Center, Nashville, TN, USA*
[2]*National Institute for Occupational Safety and Health, Cincinnati, OH, USA*

A magnetic field transduction mechanism based on an ion oscillator model is derived from an explicit quantum mechanical description. The governing equation prescribes how the electric dipole moment of an ion oscillating in a symmetric potential well evolves under the influence of an arbitrary magnetic field. The resulting equation is an analog of the Bloch equation, a well-studied model for magnetic resonances in atomic and molecular spectroscopy. The differential equation for this ion oscillator model is solved numerically for a few illustrative magnetic field exposures, showing when those resonances occur with single frequency, linearly polarized fields. Our formulation makes explicit the conditions that must be present for magnetic fields to produce observable biological effects under the ion oscillator model. The ion's potential well must have symmetry sufficient to produce a degenerate excited state, e.g., octahedral or trigonal bipyramid potentials. The impulse that excites the ion must be spatially correlated with the orientation of the detector that reads off the final state of the oscillator. The orientation between the static and oscillating magnetic fields that produces resonance is a complicated function of the field magnitudes and frequency. We suggest several classes of experiments that could critically test the validity of the model presented here. Bioelectromagnetics 25:620–630, 2004.

Key words: ion oscillator; magnetic field detection; resonance; interference

INTRODUCTION

A range of magnetic field transduction models based on an ion oscillator have been discussed in the literature on biological effects at extremely low frequencies (ELF) [Lednev, 1991; Chiabrera et al., 1992; Edmonds, 1993; Blanchard and Blackman, 1994; Binhi, 1998]. These models all capitalize on the fact that a charge moving in a magnetic field has a dynamical time scale whose natural frequency, the Larmor frequency, is determined by the field's static component, first suggested in the context of biological effects of magnetic fields by Liboff [1985]. This forms the general basis for resonant interactions when the Larmor frequency is commensurate with a periodicity in the magnetic field.

The physical model we consider is an unhydrated ion with zero electronic and nuclear spin that is oscillating in a potential well. In biology, hundreds of proteins, e.g., Ca^{2+}-calmodulin, have such bound ions. The binding potential is assumed to have sufficient symmetry for the first excited state to have two or three degenerate energy levels, and this sets very stringent restrictions on possible protein/ion candidates. In the excited state, the angular momentum of the oscillating ion induces a magnetic moment, providing a point of interaction with an external magnetic field. Posed either as a quantum mechanical or classical problem, this model has analytic solutions of the resonances when a single frequency AC field is parallel or perpendicular to the static field vector [Edmonds, 1993; Chiabrera et al., 1994; Engström, 1996; Lednev, 1996; Adair, 1998]. Generally-oriented fields should also have resonant effects, as indicated by studies of spin 1/2 systems [Ruyten, 1990a].

The resonant frequency of these ion oscillator models are half-integer multiples of γB_0 where the gyromagnetic ratio γ is one-half the ion's charge-to-mass ratio and B_0 is the static field magnitude. The magnitude of the effect is proportional to the quantity B_1/B_0, where B_1 is the peak amplitude of a time-varying sinusoidal magnetic field. These properties of the ion oscillator model have shown some consistency with

*Correspondence to: Stefan Engström, Department of Neurology Vanderbilt University Medical Center, Nashville, TN.
E-mail: stefan.engstrom@vanderbilt.edu

Grant sponsors: Holcomb Healthcare Services, LLC; Vanderbilt University.

Received for review 1 May 2003; revision received 1 December 2003

DOI 10.1002/bem.20028
Published online in Wiley InterScience (www.interscience.wiley.com).

laboratory experiments on several different biological systems [Shuvalova et al., 1991; Liboff, 1992; Blackman et al., 1994; Prato et al., 1995; Binhi, 1998; Belyaev and Alipov, 2001]. Responsiveness to B1/B0 can be explained in one of two ways: (i) the oscillating and static magnetic field components are detected separately, and their ratio is computed downstream of the component detection, (ii) the detection mechanism sees the ratio directly, implying that it operates on a time scale comparable to or greater than that of the period of the applied signal [Engström, 1997]. The latter behavior is consistent with a resonant transduction mechanism in general and with parametric resonance in particular.

Despite its empirical support, previous formulations of the ion resonance model have had theoretical problems. Adair [1992, 1998] gave several reasons why "...the model cannot account for any purported biological effect of weak extremely low frequency magnetic fields." First, ELF resonances require coherence times in the millisecond range, while thermal vibrations at biological temperatures can destroy coherence within picoseconds. Second, some theories require the potential well to be spherically symmetric, which is difficult to justify in biological molecules. Third, the degenerate excited states have to be coherent, i.e., their relative phases in an ensemble of molecules must not average to zero. Fourth, since the total amplitude of the affected dipole moment is conserved by the field, it should be impossible to detect any effects in a situation in which a spatial average over the system is considered. This study resolves the second objection by a group theory analysis of the binding site's symmetry, and deals with the two last objections by suggesting local excitation and detection mechanisms that are spatially correlated.

A further limitation of previous ion-oscillator models was that they have been solved only for the simplest exposures: a single frequency, linearly polarized AC magnetic field oriented parallel to the static field vector. A more general formalism is needed to fully test the ion oscillator model in laboratory experiments, as well as to assess exposures to ion resonance conditions from the complex magnetic fields found in the environment [Bowman and Methner, 2000]. Most experimental work based on this model concentrates on demonstrating biological dependence on the amplitude of the oscillating component. This approach assumes that a good guess of the responsible ion's properties is available, but this assumption has usually not been firmly evaluated. This is unfortunate because the fundamental resonance character of the mechanism stems from the dependence on the static field components parallel and perpendicular to the AC field. Only mapping of the system response to these static field components, as well as to the frequency of the applied field, will demonstrate the resonant character of a mechanism based on the ion-oscillator principle.

The treatment proposed below leads to a dynamic equation for the ion oscillator model that addresses some of its theoretical problems and can be applied to arbitrary magnetic fields. We will explore the consequences of this formalism for all orientations between the static and linearly polarized, single frequency magnetic fields. We thereby hope to stimulate further studies with the new range of predicted behavior.

A BLOCH EQUATION ANALOG

Our simple mathematical model consists of a singlet-triplet system where the excited state has unit angular momentum. Physically, this represents a spinless ion oscillating in a potential well. The model considers only the ion's singlet ground state and its triplet excited state, whose $L = 1$ orbital angular momentum provides a magnetic moment, similar to a hydrogen atom.

By interacting with the ion's magnetic moment, an ELF magnetic field can influence this singlet-triplet system if the unperturbed triplet's sub-levels are close enough to be mixed by the field's minute energy. For this to happen, the sub-levels must be very nearly degenerate, which requires a high degree of symmetry in the potential well. For an ion bound in a protein or other biological ligand, degenerate energy levels do not require perfect spherical symmetry in the binding potential, but can be created if the ion's nearest neighbors have rotation, reflection, and inversion symmetries that belong to a highly symmetric point group [Tinkham, 1964]. When, e.g., all the neighboring atoms are the same element and form a regular tetrahedron or octahedron, the excited states can be three-fold degenerate. Some lesser symmetries, e.g., a cube or symmetric bipyramid, produce two-fold degeneracy.

A Bloch spin-vector description is a useful tool for analyzing the dynamics of various optical and magnetic resonance phenomena. The basic Bloch equation is valid only for systems with equidistant energy levels [Hioe and Eberly, 1981; Slichter, 1990] and normally describes the evolution of a magnetic dipole moment from a 2-level (spin 1/2) system. Here we calculate the dynamics of of a $3 + 1$-level (singlet-triplet) system under the influence of a magnetic field.

It turns out that the slow (quantum beat) variation of the electric dipole moment from transitions between the excited and ground states is exactly described by an analog of the original Bloch equation (cf. Appendix):

$$\frac{d\vec{p}}{dt} = \gamma\vec{p} \times \vec{B} - \Gamma\vec{p}, \tag{1}$$

where $\vec{p}$ is a slowly varying factor of the transition electric dipole moment, modulated by the supposedly weak magnetic field $\vec{B}$. $\gamma = q/2m$ is the gyromagnetic ratio, which multiplied with the field determines the natural (Larmor) precession time scale of the quantum beats. q and m are the change and unhydrated mass of the ion, respectively. A density matrix formulation was used to calculate the time evolution of our model system (Appendix). A scalar damping term (Γ) has been added to represent the decay of excited states back to the ground state.

The full electric dipole moment ($\vec{P}$) may be reconstructed from a solution of Eq. 1 by

$$\vec{P} = \vec{p}e^{i\omega_e t} \tag{2}$$

where ω_e is the angular frequency of a ''carrier frequency'' determined by the energy separation of the first excited state and the ground state, $\omega_e = (E_1 - E_0)/\hbar$ (see Eq. 15). In our case $\omega_e \gg \Omega$, where Ω is the angular frequency of the applied field. The field only affects the slowly varying $\vec{p}$, creating interference patterns that are also called ''quantum beats.'' The excitation mechanism is left unspecified, but it must be sufficiently strong to populate the first state to a significant degree.

Analogous systems such as the magnetic moment of a two-level system that are also described by the Bloch equation, have been extensively studied with various methods [e.g., Ruyten, 1990a,b]. Reducing the system under study to this form thus opens a wealth of literature on its dynamical behavior.

INITIAL CONDITIONS AND OBSERVABLES

In a biological preparation we lack the control over the inital state that is traditionally required when studying magnetic resonance in experimental physics. In a typical setup in a physics laboratory, one would control the initial conditions by exciting states to a selected polarization and later measure only one polarization in the outgoing radiation. If this was not done, the effect of the magnetic field could not be observed for two separate reasons: (i) Since the initial state would be a randomized ensemble, rotation by the applied magnetic field would generate an equally uniform ensemble; and the field would have no observable effect. (ii) The magnitude of the electric dipole vector is conserved by the magnetic field interaction, so no effect can be observed if all components of the dipole are spatially averaged, as they would be if we summed them over all possible directions. Both these objections were raised by Adair [1992] in response to the model by Lednev [1991].

For biological systems there is a possible way out of the dilemma. If we require that the excited states are both generated and observed within the biological construct that houses the ion oscillator, we can attain correlation between the initial dipole orientation and the polarization component that is actually observed. By using local initialization and decoding of the state, we overcome the otherwise difficult problem of state preparation and polarization selection in the detector. The biological matrix which holds the oscillator may of course be expected to be randomly oriented in space, but the relative orientation of the initialization and observation can remain the same, and this is the crucial issue for this particular theoretical problem of this mechanism.

Our observable in analyzing this system will be an average of the quantum beat amplitudes p_k^2, where k indicates coordinates x,y,z. The individual instantaneous components p_k^2 are normally interpreted as the radiative probability along the corresponding (polarization) axis. Here we leave the specific biophysical interpretation open. The component response could represent a shift in charge density in the oscillator complex or a change in the probability of ion escape in a particular direction, but other interpretations may be permissible. The interaction is most likely not of a radiative nature, as indicated by Adair [1992].

The fact that the ion oscillator complex may be expected to be isotropically oriented implies that all possible orientations with respect to the applied field must be considered. In our numerical simulations below, we accomplish this by averaging the observation measures over all possible relative orientations of the field. In what follows, $\langle p_x^2 \rangle$ represents an average of p_k^2 over time (in all cases) and over all possible field orientations (except where noted).

Due to the averaging over applied field directions, there are only two independent components of the observable: parallel and perpendicular to the orientation of the initial condition vector, $\vec{p}_0$. Since p^2 is conserved by the field, these two components are proportional to one another. If we chose $\vec{p}_0 = p_0\hat{x}$ and look at the time-averaged value of p_x^2, the other two components follow from the fact that $\langle p_y^2 \rangle = \langle p_z^2 \rangle$ (there is no difference between these directions after spatial averaging) and that $\langle p^2 \rangle = \langle p_x^2 \rangle + \langle p_y^2 \rangle + \langle p_z^2 \rangle$ is unaffected by the field. The mechanisms whereby the state is prepared and decoded are thus left open with the stipulation that they be spatially correlated. The simplest way to achieve correlation would be that they belong to the same microscopic structure or even that generation and decoding is done by the same physical unit. The energy of the $L = 1$ state should substantially exceed kT, or else thermal levels will destroy the state almost instantly. Leask [1977] suggested a model which would be optically pumped. Whatever form we allow

the excitation to take, the model requires that the orientation of the excited state is correlated to the mechanism by which the final state is read.

LITERATURE OVERVIEW

In order to put our observations in context, it is useful to briefly review the literature on the ion oscillator model, paying particular attention to the treatment of initial conditions and observables.

An early idea relevant to the discussion was a suggestion by [Leask, 1977] which involved optically pumped electronic states that could be used for animal geomagnetic orientation if the emitted light could somehow be polarization-selective. Thus is the observation sensitive to a selected dipole component, but it appears that the requirement that the state be specially prepared relative to this direction is not fulfilled unless the detectors themselves are all oriented in some particular direction.

Lednev [1991] was the first to suggest using quantum beats between the Zeeman levels of an ion-oscillator perturbed by an alternating magnetic field. His observable was the probability of a radiative transition to the ion's ground state, but the method for observing the transition and for exciting the ion were not explicitly treated. Nonetheless, his derivation is implicitly consistent with our assumption of generating the exited states with the same polarization direction as the radiation detector (along a vector perpendicular to the B vector). Lednev [1991] was also the first to call this model "ion parametric resonance."

Lednev's model was criticized by Adair [1992], mainly because the states should be expected to be severely collision damped, but also for the lack of an explicit description of state initialization and observation. In reply, Lednev [1996] modified his basic model by making his observable the oscillation in a direction perpendicular to the magnetic field. Since then, the Lednev model has been further extended and critiqued [Engström, 1996; Adair, 1998].

An alternative model of the ion resonance mechanism was presented by Edmonds [1993]. The initial condition/observable treatment is implicit and basically analogous to that of Lednev.

A separate development is that of Chiabrera and co-workers [Chiabrera et al., 1992, 1994, 2000] which considers the transition behavior of a multi-level system under the influences of an external perturbation in the presence of thermal noise. They calculate the evolution of wave functions for the model and do not run into the initialization issues, but their model may be problematic in that they only consider a few low-lying energy states of the system in question.

Another take on the ion resonance idea is that of Binhi [Binghy, 1997; Bingi, 1997]. His "ion interference" mechanism explicitly includes the (fixed) initial conditions of the ion state and uses the probability of finding the ion near a particular direction as the observable. This model therefore solves the initialization/observation issue, although the isotropy of the system in the biological environment is not considered in further detail.

"Quantum interference" might be a better term for our model as well, because its effects are due to interference between the magnetically-perturbed excited states in their transition to the ground state. These interference effects do not have the same properties as the more familiar resonances in the energy transfer between two oscillating systems. Nonetheless, we choose to stick with Lednev's notion of resonance, consistent with the use of "parametric resonance" in classical mechanics for an oscillator's response to co-linear forces when the driving frequency matches the Larmor frequency [Arnold, 1973].

The modification of Lednev's model by Blanchard and Blackman [1994] was not well motivated physically, but provided explanatory power for a series of experiments [Blackman et al., 1994]. Binhi [2000] obtained the Blanchard and Blackman [1994] formulas from basic physical principles by assuming that the biological complex rotates in a highly constrained manner relative to the magnetic field.

NUMERICAL SIMULATIONS

In evaluating Eq. 1 for single frequency, linearly polarized magnetic fields, we scale the time variable $\tau = \Omega t$ and use units such that the forcing frequency and the gyromagnetic ratio equal unity: $\Omega' = \gamma' = 1$, lumping all parametric dependence into unitless magnetic flux density variables: $B' \equiv \nu$. The transformation from S.I. units to this formulation for a static field B_0 and state decay rate Γ is then:

$$B'_0 = \nu_0 = \frac{\gamma B_0}{\Omega}, \quad \Gamma' = \frac{\Gamma}{\Omega}, \tag{3}$$

where $\gamma = q/2m$ is the system's gyromagnetic ratio and Ω is the angular frequency of the oscillatory component of the applied magnetic field.

With this renormalized magnetic field, $\nu = 1$ when Ω equals the Larmor frequency of the system (γB_0). With $^{40}Ca^{2+}(\gamma = 2.41 \times 10^6\,\mathrm{C/kg})$ in a protein complex, e.g., 60 Hz is the Larmor frequency when the static field magnitude $B_0 = 2\pi(60\ Hz)/\gamma = 156.5\ \mu T \leftrightarrow \nu = 1$ in the dimensionless system. Furthermore, $\nu = 1/2$ indicates that Ω equals the system's cyclotron

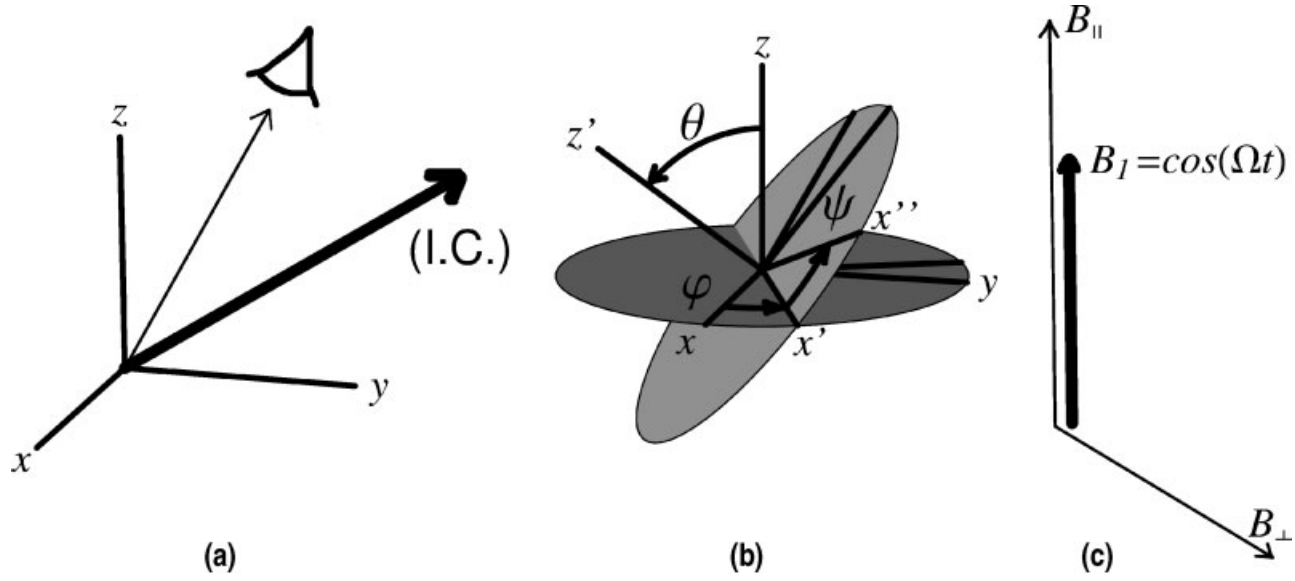

Fig. 1. Model system geometry: (**a**) The initial condition (I.C.) for the slowly varying component of the electric dipole moment $\vec{p}_0$ is defined in the same frame as the observation direction (eye). **b:** Isotropy of the ensemble of detectors is considered by uniform coverage of the three rotational degrees of freedom as described by the Euler angles (ϕ, θ, ψ). **c:** The field exposures are described by the peak amplitude of the magnetic flux density and static components parallel and perpendicular to the oscillating field.

resonance frequency; $\nu_{\|} = n/2$ and $\nu_{\perp} = 0$ represents the parametric resonance condition; etc.

We now consider three renormalized magnetic field variables: ν_1, $\nu_{\|}$, and $\nu_{\perp}$, corresponding to the oscillating, static parallel, and static perpendicular components, respectively. Without loss of generality we let the oscillating component lie along the $\hat{z}$ axis and we get (cf. Fig. 1c):

$$\frac{d\vec{p}}{d\tau} = \vec{p} \times ((\nu_1 \cos\tau + \nu_{\|})\hat{z} + \nu_{\perp}\hat{x}) - \Gamma'\vec{p}. \quad (4)$$

We will choose the initial conditions to be $\vec{p}_0 = \hat{x}$. In the course of numerically integrating $\vec{p}$ we also calculate the integral of p_x^2, the time average of which will represent the observable quantity that eventually propagates through a biological signal pathway and becomes accessible to experimentation.

The normalization of the calculated $\vec{p}$ was based on the following observation. After scalar multiplication of Eq. 1 with $\vec{p}$, we find that, since $2\vec{p} \cdot d\vec{p}/dt = dp^2/dt$ and, for any vector $\vec{q}$, $\vec{p} \cdot \vec{p} \times \vec{q} = 0$:

$$\frac{dp^2}{dt} = -2\Gamma' p^2. \quad (5)$$

It follows that the amplitude of $\vec{p}$ is unaffected by the magnetic field and declines only due to the damping term. Therefore, the individual components are normalized by the integral of the component sum ($1/2\Gamma'$ for a sufficiently long integration) in order to allow direct comparison of simulations with different Γ'.

When calculating the effect of having an isotropic ensemble of detectors (Fig. 1a), we need to average our results over a set of rotations of the detector system. We accomplish an equivalent operation by instead averaging p_x^2 over a set of rotations of the field vectors. The applied fields are rotated by Euler angles ϕ, θ, ψ, where (ψ, θ) are chosen to uniformly sample the unit sphere in $n_{\phi\theta}$ segments and the range for ψ is divided into n_{ψ} equal intervals (cf. Fig. 1b). This gives the temporal and spatial average of the detected dipole moment $\langle p_x^2 \rangle$, the observable quantity in our model biological system. Typical parameters used in our calculations are given in Table 1.

RESULTS

The resonant structure resulting from Eq. 1 has been extensively studied in the literature (see Ruyten [1990a] and references therein). Best known are the responses of the Bloch equation to parallel and perpendicular magnetic field combinations, as shown by time traces of $\vec{p}$ from the numerical integration of Eq. 4 (Fig. 2). With parallel fields, the oscillating dipole vector precesses in the plane perpendicular to the fields, while the perpendicular field creates motion along the z axis. With most field combinations, the dipole's oscillations over infinite time are directed in all possible

TABLE 1. Numerical Simulation Parameters

Parameter	Value	Comment
Γ'	.05	Damping factor
θ_0	$\pi/2$	Initial condition for $\vec{p}$
ϕ_0	0	$\vec{p}_0 = (\sin(\theta_0)\cos(\phi_0),\ \sin(\theta_0)\sin(\phi_0),\ \cos(\theta_0))$
n_{per}	10	Number of periods to evaluate
$n_{\theta\phi}$	120	Subdivision of the sphere for (θ, ϕ)-isotropy
n_ψ	10	Number of ψ segments considered
ν_1	0–4	Dimensionless oscillating field amplitude
$\nu_\parallel$	0–4	Static field amplitude parallel to ν_1
$\nu_\perp$	0–4	Static field amplitude perpendicular to ν_1

''Value'' represents typical parameters in a simulation. Unless otherwise noted in text and figures, these are the values used in the reported simulations.

angles. The resonant fields, however, focus the oscillation toward or away from the detector, creating anisotropy in the average electric dipole. Resonant parallel fields $\nu_\parallel = 1.0$ create trajectories for $\vec{p}$ that are C-shaped with their 67.4° openings all aligned along the x axis. This focuses the electric dipole more along the y axis, the defining characteristic of parametric resonance. In contrast, non-resonant parallel fields also produce C-shaped trajectories, but their openings are not aligned, making the dipole's distribution more isotropic. With perpendicular fields, the oscillations in the resonant case nutate back and forth across the binding site's ''equator,'' never exceeding 35° in latitude. With non-resonant fields, the dipole crosses the ''poles'' creating greater isotropy. This same nutation is found in the resonance of spin 1/2 magnetic moments familiar from NMR, ESR and MRI [Slichter, 1990]. These differences in anisotropy can also be seen in the plots of $\langle p_x^2 \rangle$ for parallel, perpendicular, and mixed magnetic field combinations (Figs. 3–7).

The simulations of our model differ from most other work in that we have generally considered all possible orientations of the field vector relative to the detector. This is not expected to radically change the main features of the response, as our results confirm, but differences in details reflect our consideration of detector isotropy.

Figure 3 displays the results of varying the static field components parallel ($\nu_\parallel \in [0,4]$) and perpendicular ($\nu_\perp \in [0,4]$) to a fixed-amplitude sinusoidal vector ($\nu_1 = 4$), allowing a direct comparison to Figure 10 in Ruyten [1990a]. Much of the structure predicted by continued fraction analysis of the same underlying equation is retained in our isotropically averaged version. There are parametric resonances for $\nu_\perp = 0$, Haroche resonances for $\nu_\parallel = 0$. Away from the $\nu_\parallel = 0$ and $\nu_\perp = 0$ axes, there are only a few fixed Haroche-like resonances (a type of level-crossing resonance) in the $(\nu_\parallel, \nu_\perp)$ plane [Yabuzaki et al., 1974]. Level crossing refers to a matching of energy levels and a possibility of state interchange, due to magnetic field interactions. As the stimulus amplitude (ν_1) is varied, the crests and troughs of the response will ripple through this plane, providing a large space of possible experimental predictions.

Damping is represented by a single time scale ($\tau_{damp} = 1/\Gamma'$) in our model. This simple model exhibits the expected Lorentzian-shaped parametric resonances for a range of Γ' as seen in Figure 4. This parameter has a relatively small range of possible values for which one can hope to observe the effects of an ion-oscillator based mechanism in biological systems. If Γ' exceeds approximately 1/2, then the oscillator is damped out rapidly and no resonance can be observed. As the damping parameter approaches zero, the resonances become increasingly narrow, and consequently more difficult to detect unless one has very precise information about the frequency required for resonance.

Experimental Implications

The following observations on our results provide some testable hypotheses for a critical experimental evaluation of this model:

The introduction of spatial averaging has a relatively small impact on the qualitative predictions for the condition of parallel static and oscillating fields. The locations of resonances at half-integer $\nu_\parallel$ are not affected by the relative orientation of field and detector or by the strength of the applied oscillating amplitude [Ruyten, 1990a], as shown in Figures 4 and 5, which show parametric resonances for two different forcing amplitudes ($\nu_1 = 1$ and 4, respectively).

When the static field is perpendicular to the oscillating field, another set of resonances are seen. In particular, there is a response to relatively weak oscillating fields as shown in Figure 6. The precise location of the resonance peaks will generally vary with the strength of the oscillating field (ν_1), although there exist stationary resonances in this (and the mixed parallel/perpendicular) case as well. An observation of the feature depicted in Figure 6 for a small perturbation amplitude (ν_1) would provide a nice contrast to the expected behavior of a model which depends solely on the field amplitude, such as a geminate free radical pair model responding to low frequency magnetic fields in an isotropic system. The reason is that a model which depends on the amplitude would not easily discriminate a small perpendicular component, since if $B_1 \ll B_0$ we have that root-mean-squared magnitude $|B| = \sqrt{B_0^2 + B_1^2} \approx B_0(1 + x^2/2)$, where $x = B_1/B_0$.

Another way to generate model predictions for the outcomes of combined parallel and perpendicular static

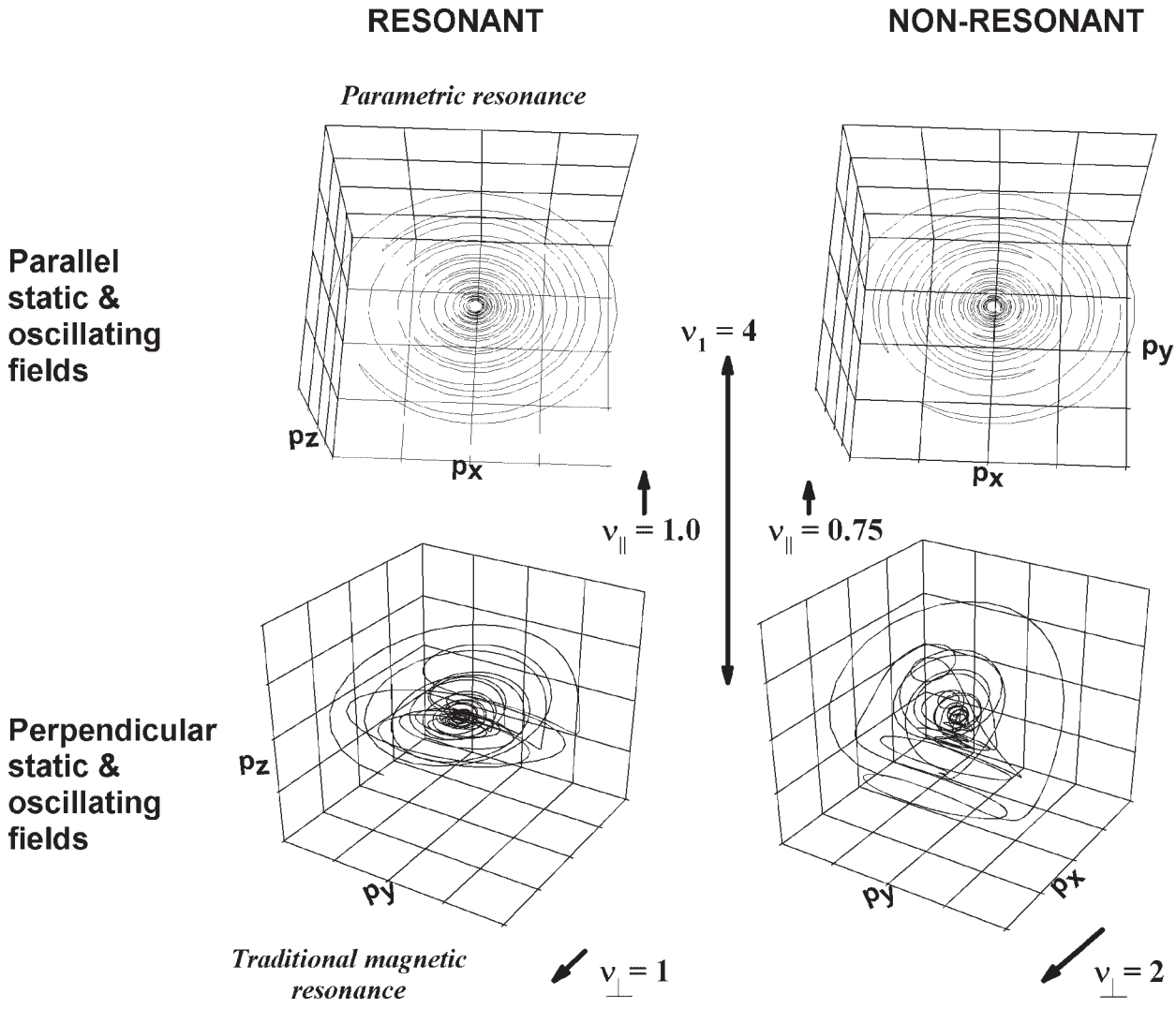

Fig. 2. Traces of the slowly varying factor $\vec{p}$ of the electric dipole moment vector $\vec{p}$ (Eq. 2) in response to four combinations of the static and oscillating magnetic fields: parallel ($\nu_\perp = 0$) vs. perpendicular ($\nu_\parallel = 0$) and resonant vs. non-resonant. All traces are calculated with a time period $\Delta\tau = 60$ and a damping parameter $\Gamma' = 0.05$. Note that this is not the full dipole vector $\vec{P}$, which oscillates rapidly through the origin while following the trajectory of $\vec{p}$.

components is to follow the response in $\langle p_x^2 \rangle$ along the ray $\nu_\parallel = \nu_\perp$ as seen in Figure 7. In this example, which summarizes a small range of oscillating amplitudes ($\nu_1 \in [1.4,\ 1.8]$), we see a relatively stationary structure which could provide experimental support for (or rejection of) this model.

Further experimental tests of this model are provided by its postulates. Consider first the zero spin condition. This is a necessary postulate for obtaining the Bloch-type equation because either electron or nuclear spins will split the ground and excited states, producing a much larger density matrix and more complicated result. Zero electron spin can be achieved by requiring closed electronic shells, which are found in many biologic ions. Far rarer are biologic ions with both zero electronic and nuclear spins in their most abundant isotopes: $^{24}Mg^{2+}$ (80.0% abundance), $^{26}Mg^{2+}$ (11.0%),^{40} Ca^{2+} (96.9%), $^{44}Ca^{2+}$ (2.1%), $^{64}Zn^{2+}$ (48.6%), $^{66}Zn^{2+}$(27.9%), and $^{68}Zn^{2+}$(18.8%). Therefore, the magnetic resonance responses predicted in Figures 3–7 can only be displayed by biologic complexes of magnesium, calcium, and zinc. (Note the γ values of the natural magnesium and zinc isotopes vary by 6–8%, which will slightly broaden any observed resonances.)

The model's symmetry requirements impose further constraints on the biological substrates. Although magnesium, calcium and zinc are bound by hundreds of proteins with up to a dozen ions per protein [McPhalen et al., 1991; Alberts et al., 1998], the atoms from surrounding amino acid and water molecules generally

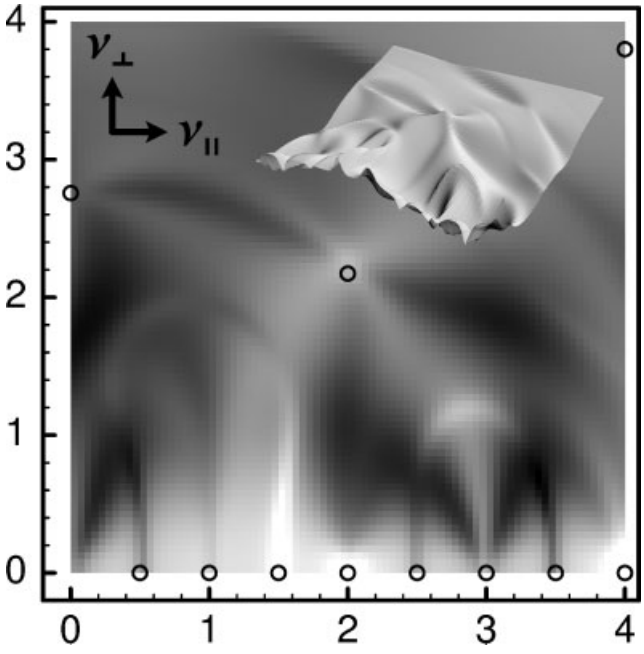

Fig. 3. Response structure of the Bloch-type equation as a function of parallel ($\nu_{||}$) and perpendicular ($\nu_\perp$) field components for a fixed oscillating amplitude of $\nu_1 = 4$. The gray-scale corresponds to values in the observable $\langle p_x^2 \rangle$, with black-to-white representing increasingly larger values. Parametric ($\nu_\perp = 0$), Haroche ($\nu_{||} = 0$) and Haroche-like ($\nu_\perp > 0$, $\nu_{||} > 0$) resonances are marked with circles in the figure. The location of parameteric resonances are independent of the strength of the oscillating field (ν_1), while the location in $\nu_\perp$ of Haroche and Haroche-like resonances depend on this parameter. The inset image is a 3D view of the same information $\Gamma' = 0.05$.

form an irregular polygon with less symmetry than the resonance model requires. McPhalen et al., 1991 analyzed the geometry of 77 calcium-binding sites in 28 well-studied proteins, including Ca^{2+}-calmodulin.

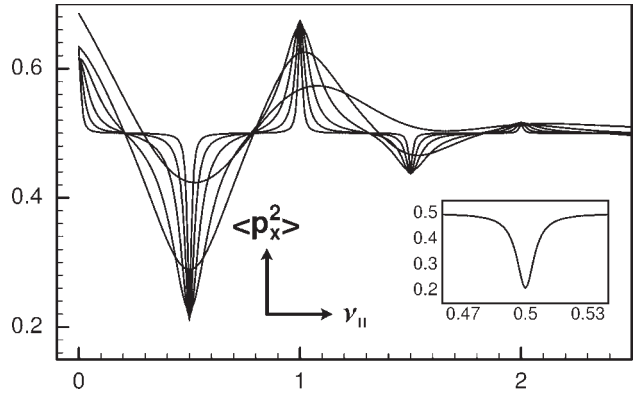

Fig. 4. The effect of damping on the response in $\langle p_x^2 \rangle$ at the parametric resonance condition: $\nu_{||} \in [1, 2.5]$, $\nu_\perp = 0$, $\nu_1 = 1$. The damping parameter takes the values $\Gamma' \in \{0.010, 0.025, 0.050, 0.100, 0.250, 0.500\}$. Wider resonances correspond to larger values of Γ'. The inset panel shows a close-up of the $\nu_{||} = 1/2$ resonance for $\Gamma' = 0.005$.

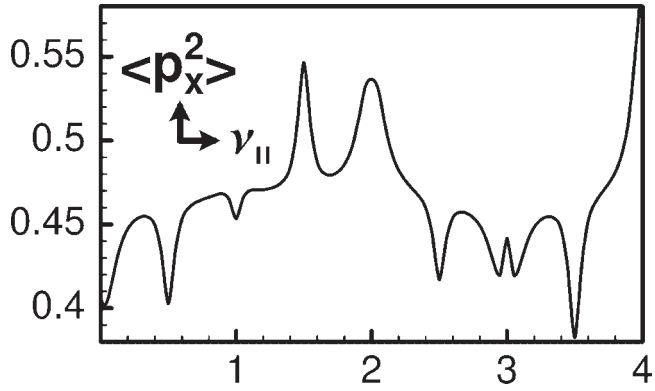

Fig. 5. The figure shows the response in $\langle p_x^2 \rangle$ to $\nu_{||} \in [0, 4]$ for $\nu_1 = 4$ with damping $\Gamma' = 0.05$.

Based on X-ray crystallography, these binding sites have 5–8 neighboring oxygen atoms, but none formed an ideal octahedron. Only one calcium-binding site on the protein α-Lactalbumin might be an ideal pentagonal bipyramid within crystallography's 4–8% error bounds (.1–.2 Å precision for Ca^{2+}-ligand bond distances averaging 2.4 Å). Based on this limited survey, most proteins with spin zero ions do not have the symmetry required for ion magnetic resonance, but a few might. A systematic geometric analysis of the structures in the online Protein Data Bank [Berman et al., 2000] might provide additional candidates for the magnetic resonance experiments proposed here.

DISCUSSION

Amplitude windows are a recurring (and disputed) observation in the field of bioelectromagnetics [Shuvalova et al., 1991; Blackman et al., 1994; Prato et al., 1995; Binhi, 1998; Belyaev and Alipov, 2001]. Lednev's ion-oscillator model demonstrated a possible mechanism for obtaining these otherwise problematic observations. This work extends the Lednev model to consider arbitrary exposure conditions instead of only parallel static and sinusoidal oscillating magnetic fields.

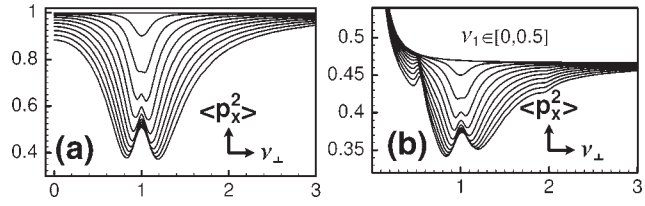

Fig. 6. Magnetic resonance ($\nu_{||} = 0$, $\nu_\perp = 0 - 3$) for a range of relatively weak oscillating field amplitudes: $\nu_1 \in [0, 0.5]$ in steps of $\Delta\nu = 0.05$. The top curve corresponds to $\nu_1 = 0$ and descending curves indicate larger values of ν_1. **a:** Shows the single orientation case where a single detector/field orientation has been considered. **b:** A similar calculation averaged over all orientations exhibits a similar structure, but the details of the observable ($\langle p_x^2 \rangle$) is changed. $\Gamma' = 0.05$.

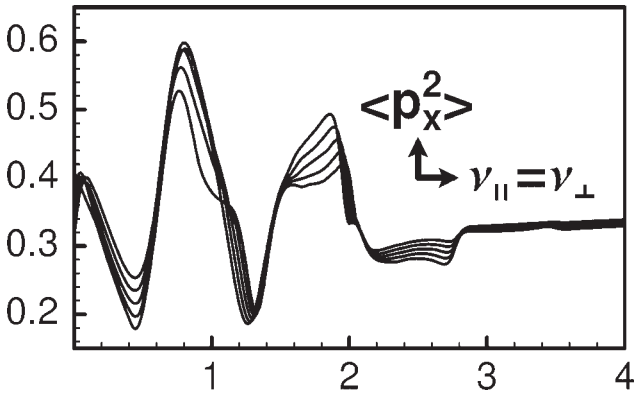

Fig. 7. A diagonal section along the ray $\nu_{\|} = \nu_{\perp}$ shows some of the combined-field resonant structures. In this case $\nu_{\|} = \nu_{\perp} \in [0, 4]$ and ν_1 takes a few values in the range [1.4,1.8]. $\Gamma' = 0.05$.

To see the equivalence with the Lednev formalism, examine the single frequency version of the Bloch equation (Eq. 4) with $\nu_{\perp} = 0$ and no damping ($\Gamma' = 0$). This gives $\dot{p}_{\pm} = \mp i\omega(\tau)p_{\pm}$ where $p_{\pm} = (p_x \pm ip_y)/\sqrt{2}$ and $\omega(\tau) = \nu_1 \cos\tau + \nu_{\|}$. Integrating this differential equation and comparing it with Lednev [1991] shows that the electric dipole components $p_{\pm}$ are proportional to his ''electromagnetic field amplitudes'' for states 1 and 2, which are the $L = 1$, $M = \pm 1$ states in our formulation or the right/left-handed circular orbits in the classical treatment by Adair [1998]. Furthermore, $p_x^2 = \frac{1}{2}|p_+ + p_-|^2$ is proportional to Lednev's ''probability of transition to the ground state'' and the ''ion-protein dissociation probability'' in Binghy [1997b]. The integral of p_x^2 over time therefore gives their parametric resonance equations, as our numerical simulation confirms (Fig. 5).

The most plausible physical interpretation for how $\langle p_x^2 \rangle$ might affect biological systems is through ion-protein dissociation. Altered rates of ion dissociation from a protein could have biological effects because bound ions can impact the protein's enzymatic properties or the stability of its folds, as in α-Lactalbumin [McPhalen et al., 1991]. However, $\langle p_x^2 \rangle$ can have an impact on dissociation only if there is an opening (or gate) in the potential well along the x axis, which is aligned opposite to negatively-charged ligand atoms. Furthermore, Adair [1998] points out that the potential well openings must maintain the same high symmetry if resonance is to occur, and $\langle p_x^2 \rangle$ obviously does not have this symmetry. However, we could postulate a protein complex with multiple gates aligned symmetrically, such as a pentagonal bipyramid with five gates around the base. Binhi [2000] discusses further properties of the dissociation process qualitatively. Clearly, a comprehensive ion-oscillator model should include a mathematical dissociation mechanism.

A similar model may be generated for the slightly less demanding case of two-fold symmetry instead of the three-fold case we have investigated in this article. This system would only respond to the field component perpendicular to the symmetry plane. Modeling this system mathematically becomes more laborious since the creation of an additional reference orientation that has to be considered in relation to the detector/observable complex while performing the averaging over all possible field orientations.

The second important feature of the present formulation is how the oscillator's initial conditions and the system observable must be spatially correlated in order to observe an effect, particularly in a situation in which the ensemble of biological detectors are isotropically distributed in space. As discussed in the ''Initial Conditions and Observables,'' this spatial correlation would be achieved if both the excitation as well as the detection are done by the ligand binding site. Such an excitation could be achieved by one of the ligand atoms when the protein is refolding.

Our treatment does provide solutions for the initial condition and symmetry problems of the ion oscillator model [Adair, 1992, 1998], but severe obstacles still remain before this approach will achieve physical acceptance. Experimental studies have focused on applying fields with frequencies primarily in the range 1–1000 Hz, indicating resonant time scales measured in milliseconds. An interaction which requires coherence times in the millisecond range is not an attractive feature of a quantum mechanical explanation of a system at biological temperatures. The idea of molecular gyroscopes may provide a framework for solving this dilemma [Binhi and Savin, 2002]. Creating state coherence and its maintenance under thermal perturbations are difficult issues for this type of model. Nonetheless, very long coherence times appear unavoidable if we wish to entertain the idea of a resonance-based solution with molecular-sized constituent elements.

REFERENCES

Adair RK. 1992. Criticism of Lednev's mechanism for the influence of weak magnetic fields on biological systems [comment]. Bioelectromagnetics 13(3):231–235.

Adair RK. 1998. A physical analysis of the ion parametric resonance model. Bioelectromagnetics 19:181–191.

Alberts IL, Nadassy K, Wodak SJ. 1998. Analysis of zinc binding sites in protein crystal structures. Protein Sci 7:1700–1716.

Arnold VI. 1973. Ordinary differential equations. Cambridge: MIT Press.

Belyaev IY, Alipov ED. 2001. Frequency-dependent effects of elf magnetic field on chromatin conformation in *Escherichia coli* cells and human lymphocytes. Biochim Biophys Acta-Gen Subj 1526:269–276.

Berman HM, Westbrook J, Feng Z, Gilliland G, Bhat TN, Weissig H, Shindyalov IN, Bourne PE. 2000. The protein data bank. Nucleic Acids Res 28:235–242.
Binghy VN. 1997. Interference of ion quantum states within a protein explains weak magnetic field's effect on biosystems. Electro Magnetobiol 16:203–214.
Bingi VN. 1997. The mechanism of magnetosensitive binding of ions by some proteins. Biophysics 42:317–322.
Binhi VN. 1998. Interference mechanism for some biological effects of pulsed magnetic fields. Bioelectrochem Bioenerg 45(1):73–81.
Binhi VN. 2000. Amplitude and frequency dissociation spectra of ion–protein complexes rotating in magnetic fields. Bioelectromagnetics 21:34–45.
Binhi VN, Savin AV. 2002. Molecular gyroscopes and biological effects of weak extremely low-frequency magnetic fields. Phys Rev E Stat Nonlin Soft Matter Phys 65:051912.
Blackman CF, Blanchard JP, Benane SG, House DE. 1994. Empirical test of an ion parametric resonance model for magnetic field interactions with PC-12 cells. Bioelectromagnetics 15(3):239–260.
Blanchard JP, Blackman CF. 1994. Clarification and application of an ion parametric resonance model for magnetic field interactions with biological systems. Bioelectromagnetics 15(3):217–238. Erratum appears in Bioelectromagnetics 1994;155:493.
Bowman JD, Methner MM. 2000. Hazard surveillance for industrial magnetic fields: Ii. field characteristics from waveform measurements. Ann Occup Hyg 44:615–633.
Chiabrera A, Bianco B, Tommasi T, Moggia E. 1992. Langevin–Lorentz and Zeeman–Stark models of bioelectromagnetic effects. Acta Pharm 42:315–322.
Chiabrera A, Bianco B, Moggia E, Tommasi T. 1994. Interaction mechanism between electromagnetic fields and ion adsorption—Endogenous forces and collision frequency. Bioelectrochem Bioenerg 35(1–2):33–37.
Chiabrera A, Bianco B, Moggia E, Kaufman JJ. 2000. Zeeman–Stark modeling of the RF EMF interaction with ligand binding. Bioelectromagnetics 21:312–324.
Edmonds DT. 1993. Larmor precession as a mechanism for the detection of static and alternating magnetic fields. Bioelectrochem Bioenerg 30:3–12.
Engström S. 1996. Dynamic properties of Lednev's parametric resonance mechanism. Bioelectromagnetics 17(1):58–70.
Engström S. 1997. What is the time scale of magnetic field interaction in biological systems? Bioelectromagnetics 18(3): 244–249.
Hioe FT, Eberly JH. 1981. N-level coherence vector and higher conservation laws in quantum optics and quantum mechanics. Phys Rev Lett 47(12):838–841.
Leask MJM. 1977. A physicochemical mechanism for magnetic field detection by migratory birds and homing pigeons. Nature 267(5607):144–145.
Lednev VV. 1991. Possible mechanism for the influence of weak magnetic fields on biological systems [see comments]. Bioelectromagnetics 12(2):71–75.
Lednev VV. 1996. Bioeffects of weak static and alternating magnetic fields. Biofizika 41:224–232.
Liboff AR. 1985. Cyclotron resonance in membrane transport. In: Chiabrera A, Nicolini C, Schwan HP, editors. Interactions between electromagnetic fields and cells. London, UK: Plenum Press.
Liboff AR. 1992. The cyclotron resonance hypothesis: Experimental evidence and theoretical constraints. In: Nordén B, Ramel C, editors. Interaction mechanisms of low-level electromagnetic fields in living systems. Oxford, UK: Oxford University Press. pp 130–147.
McPhalen CA, Stynadka NCJ, James MNG. 1991. Calcium-binding sites in proteins: A structural perspective. Adv Phys Chem 42:77–144.
Prato FS, Carson JJ, Ossenkopp KP, Kavaliers M. 1995. Possible mechanisms by which extremely low frequency magnetic fields affect opioid function. Faseb J 9(9):807–814.
Ruyten WM. 1990a. Magnetic and optical resonance of two-level quantum systems in modulated fields. i. bloch equation approach. Phys Rev A Atomic Mol Opt Phys 42(7):4226–4245.
Ruyten WM. 1990b. Magnetic and optical resonance of two-level quantum systems in modulated fields. ii. floquet hamiltonian approach. Phys Rev A Atomic Mol Opt Phys 42(7):4246–4254.
Shuvalova LA, Ostrovskaya MV, Sosunov EA, Lednev VV. 1991. The effect of a weak magnetic field in the paramagnetic resonance mode on the rate of the calmodulin-dependent phosphorylation of myosin in solution. Doklady Akademii Nauk Sssr 317(1):227–230.
Slichter CP. 1990. Principles of magnetic resonance/; SE Springer series in solid-state sciences; 1. 3rd and updated edn. Berlin, New York: Springer-Verlag.
Tinkham M. 1964. Group theory and quantum mechanics. New York: McGraw-Hill.
Yabuzaki T, Nakayama S, Murakami Y, Ogawa T. 1974. Interaction between a spin-1/2 atom and a strong rf field. Phys Rev A 10(6):1955–1963.

APPENDIX

Derivation of the Bloch Analog Equation

The Hamiltonion operator ($\mathcal{H}$) for a spinless particle whose orbital angular momentum $\vec{\mathcal{L}}$ interacts with a magnetic field (magnetic flux density $\vec{B}$) is:

$$\mathcal{H} = \mathcal{H}_0 - \frac{q}{2m}\vec{B}\cdot\vec{\mathcal{L}}, \tag{6}$$

where q and m are the particle's charge and mass, $\mathcal{H}_0$ is the unperturbed Hamiltonian.

Assume that the particle's energy is low enough to populate only the ground state (quantum number $L=0$, energy E_0) and first-excited state ($L=1$, E_1). Further, the excited state is three-fold degenerate ($M=0,\pm 1$) because of the potential well's symmetry. Group theory shows that this three-fold degeneracy is found in the excited states of particles bound by potentials whose symmetry operations form the tetrahedral or octahedral point group [Tinkham, 1964].

Now consider an ensemble of N ion oscillators, e.g., all the ions in a cell which are bound at a particular site in a protein. If these oscillators are non-interacting, the ensemble's quantum properties can be represented by its density matrix $\mathcal{D} = \{D_{ij}\} \equiv 1/N \sum_{n=1}^{N} a_{ni}^{*} \,|\, ni > < nj \,|\, a_{nj}$ where a_{ni} is the coefficient for the time dependence of the i-th state $|ni>$ of the n-th oscillator.

In our model, the density matrix and all other operators are 4×4 matrices with indices $i, j = 1,2,3,4 \leftrightarrow \{L,M\} = \{1,-1\},\{1,0\},\{1,+1\},\ \{0,0\}$. The time evolution of the density matrix is described by:

$$\dot{\mathcal{D}} = \frac{1}{i\hbar}[\mathcal{H},\mathcal{D}]. \tag{7}$$

Using the $L=1$ matrix elements for the angular momentum operator [Slichter, 1990], the Hamiltonian matrix for this 4-state system is:

$$\mathcal{H} = \begin{pmatrix} E_1+\hbar\omega_z & -\hbar\omega_+ & 0 & 0 \\ -\hbar\omega_- & E_1 & -\hbar\omega_+ & 0 \\ 0 & -\hbar\omega_- & E_1-\hbar\omega_z & 0 \\ 0 & 0 & 0 & E_0 \end{pmatrix}, \tag{8}$$

where

$$(\omega_x,\omega_y,\omega_z) = \vec{\omega} = \frac{q}{2m}\vec{B}(t),\ \text{and}\ \omega_\pm = (\omega_x \pm i\omega_y)/\sqrt{2}. \tag{9}$$

Our observable is the electric dipole moment, $\vec{\mathcal{P}} = q\vec{\mathcal{R}}$, which has the following matrix representation:

$$\mathcal{P}_x = qr\begin{pmatrix} 0&0&0&1\\0&0&0&0\\0&0&0&-1\\1&0&-1&0\end{pmatrix}$$

$$\mathcal{P}_y = q_r\begin{pmatrix} 0&0&0&i\\0&0&0&0\\0&0&0&i\\-i&0&-i&0\end{pmatrix}$$

$$\mathcal{P}_z = \sqrt{2}qr\begin{pmatrix} 0&0&0&0\\0&0&0&1\\0&0&0&0\\0&1&0&0\end{pmatrix},$$

where qr is the charge times a characteristic radius of the oscillator [Slichter, 1990].

The expectation value of the dipole moment is

$$\vec{P} = \mathrm{Tr}[\mathcal{D}\vec{\mathcal{P}}]. \tag{10}$$

Since $\mathcal{D}$ is Hermitian we find that:

$$\begin{aligned} P_x &= 2qr\mathrm{Re}[D_{14}-D_{34}] \\ P_y &= 2qr\mathrm{Im}[D_{14}+D_{34}] \\ P_z &= 2\sqrt{2}qr\mathrm{Re}[D_{24}]. \end{aligned} \tag{11}$$

Next we define auxiliary operators ($\mathcal{P}_1$, $\mathcal{P}_2$, $\mathcal{P}_3$) forming a complete description of the relevant density matrix components. They are chosen such that their expectation values are:

$$\begin{aligned} P_1 &= -2qr\mathrm{Im}[D_{14}-D_{34}] \\ P_2 &= 2qr\mathrm{Re}[D_{14}+D_{34}] \\ P_3 &= -2\sqrt{2}qr\mathrm{Im}[D_{24}]. \end{aligned} \tag{12}$$

Only three components of the matrix differential equation Eq. 7 contribute to the evolution of the chosen operator variables. The corresponding dynamical equations can be obtained by applying the commutator Eq. 7 the model's Hamiltonian Eq. 8:

$$\begin{aligned} \dot{D}_{14} &= (i\omega_x D_{24} - \omega_y D_{24})/\sqrt{2} - i\omega_z D_{14} - i\omega_e D_{14} \\ \dot{D}_{34} &= (i\omega_x D_{24} + \omega_y D_{24})/\sqrt{2} + i\omega_z D_{34} - i\omega_e D_{34} \\ \dot{D}_{24} &= (i\omega_x(D_{14}+D_{34}) + \omega_y(D_{14}-D_{34}))/\sqrt{2} - i\omega_e D_{24}, \end{aligned} \tag{13}$$

where $\omega_e = (E_1 - E_0)/\hbar$.

Writing Eq. 13 in terms of operator variables using Eqs. 11 and 12, we obtain:

$$\begin{aligned} \dot{P}_x &= \omega_z P_y - \omega_y P_z - \omega_e P_1 \\ \dot{P}_y &= -\omega_z P_x + \omega_x P_z - \omega_e P_2 \\ \dot{P}_z &= \omega_y P_x - \omega_x P_y - \omega_e P_3 \\ \dot{P}_1 &= \omega_z P_2 - \omega_y P_3 + \omega_e P_x \\ \dot{P}_2 &= -\omega_z P_1 + \omega_x P_3 + \omega_e P_y \\ \dot{P}_3 &= \omega_y P_1 - \omega_x P_2 + \omega_e P_z. \end{aligned} \tag{14}$$

Express $\vec{P}$ and the corresponding auxiliary variables in terms of a slowly varying part, p_α.

$$P_\alpha = p_\alpha e^{i\omega_e t}, \quad \alpha = x,y,z,1,2,3. \tag{15}$$

$$P_\alpha = (\dot{p}_\alpha + i\omega_e p_\alpha)e^{i\omega_e t}. \tag{16}$$

After canceling the common term $\exp(i\omega_e t)$, the equations for p_α are those of P_α with an extra term $-i\omega_e p_\alpha$ added to the RHS. Finally, consider the dynamical equations for the complex variables: $p_x + ip_1$, $p_y + ip_2$, and $p_z + ip_3$:

$$\begin{aligned} \dot{p}_x + i\dot{p}_1 &= \omega_z p_y - \omega_y p_z + i(\omega_z p_2 - \omega_y p_3) \\ \dot{p}_y + i\dot{p}_2 &= -\omega_z p_x + \omega_x p_z + i(-\omega_z p_1 + \omega_x p_3) \\ \dot{p}_z + i\dot{p}_3 &= \omega_y p_x - \omega_x p_y + i(\omega_y p_1 - \omega_x p_2). \end{aligned} \tag{17}$$

Eq. 17 separates the equations for p_{xyz} from those for p_{123} and they can therefore be solved independently. Since Eq. 15 connects p_{xyz} directly to the physical variables P_{xyz}, we know this is the quantity of physical interest. This final result can be re-written as a Bloch equation analog:

$$\dot{\vec{p}} = \vec{p}\times\vec{\omega} = \gamma\vec{p}\times\vec{B}(t), \tag{18}$$

where $\vec{p} = (p_x, p_y, p_z)$ and $\gamma = q/2m$.